Zhiyuan Chen, Lijun Wang*, Fushen Li and Kuochih Chou

Thermodynamic Analysis of the Corrosion of Fe-16Cr Alloy Interconnect of Solid Oxide Fuel **Cell under Various Atmospheres**

Abstract: Iron-based alloys are the most hopeful interconnects of intermediate temperature solid oxide fuel cell (IT-SOFC). Fe-16Cr alloy is one of the common iron-based alloys. Oxidation of the alloy is the key issue in the running process, which could be described in terms of diffusion path. Chemical potential, which is one of the primary factors to the diffusion process, is determined by the thermodynamics. The equilibrium phase in the oxidation of Fe-16Cr alloy was analyzed for better understanding of the mechanism of alloy oxidation in varied atmosphere. A novel form of thermodynamic diagram associated to the oxidation process was given. Phases in the equilibrium are changing with the quantitative increase of reacted fuel gas during the process. The diagram of Fe-16Cr alloy in atmospheres at cathode and anode sides were calculated. The diagram gives the intuitionistic phase transformation process corresponding to the practical oxidation process in the view of thermodynamics.

Keywords: stainless steel, interconnect, solid oxide fuel cell, oxidation, corrosion, equilibrium

PACS® (2010). 64.70.kd, 05.70.Fh

*Corresponding author: Lijun Wang: School of Metallurgical and Ecological Engineering, University of Science and Technology Beijing, Beijing 100083, China. E-mail: lijunwang@ustb.edu.cn Zhiyuan Chen, Kuochih Chou: School of Metallurgical and Ecological Engineering, University of Science and Technology Beijing, Beijing 100083, China Fushen Li: School of Material Science Engineering, University of

Science and Technology Beijing, Beijing 100083, China

1 Introduction

The interconnect of an solid oxide fuel cell (SOFC) stack electrically and physically connects the anode of one fuel cell to the cathode of the adjacent fuel cell in the stack. The interconnect can be ceramic or metallic materials. Considering the economical use in SOFC stacks, metallic interconnects are more promising materials, such as iron-based alloys, nickel-based alloys as well as chromium-based alloys [1–5]. It is easy to notice all these materials contain chromium since it is one of most important anti-corrosion elements. Among these metallic materials, ferritic stainless steel can be regarded as the most economical one for the interconnection of SOFC. Commonly, it contains 10-30% Cr and a small amount of Mn [3].

The interconnect materials used for SOFC stacks must be oxidation resistant, impermeable to the diffusion of gases, and chemically stable with fuel cell materials. Furthermore, the oxide scale formed should not spall from the substrate. In case of the oxidation resistant, a number of investigations were carried out in both air and fuel atmospheres [6–20]. The oxidates formed in the oxidation process of ferritic stainless steel were found in sequence. The Cr-basedoxide was formed on the surface of the stainless steel at initial. Take Fe-16Cr alloy for example; a double layered oxide scale was formed in this stage. The outside layer was MnCr₂O₄, and the next layer was Cr₂O₃. With oxidation continued, FeCr₂O₄ was observed. If the reaction time was long enough, ferriferous oxide would also formed [13, 14]. The sequence of oxides formation can be attributed to elements diffusion capacities, different physical properties of oxides and also oxidation thermodynamics. Diffusion kinetics is the determining factor of the scale forming ways. However, Chemical potential of oxide is one of the keys of the diffusion path in the stainless steel oxidation, which could be calculated in thermodynamics. Equilibrium diagrams and Ellingham charts interrelated with the oxidation was provided in many reports [11–14, 21, 22]. However, there are few of thermodynamic analysis associated to the practical alloy-gas system but pure substances only.

Equilibrium calculation of Fe-16Cr alloy oxidation was performed in anode and cathode atmospheres in the current work. A novel form of thermodynamic diagram was given. Change process of compounds amounts in the oxidation of Fe-16Cr alloy were quantification in the series of diagrams. The effects of temperature, chromium content and atmosphere to the oxidation were considered.

Table 1: Chemical composition of Fe-16Cr alloy.

Elements	С	Si	Cr	Ni	Mn	S	Р
mass%	0.05	0.40	16.05	0.05	0.25	0.005	0.012

2 Thermodynamic calculation

The thermodynamic calculation was performed in Gibbs energy minimizer of ChemSage Module of FactSage 6.2 with the database of FACT53. There is no data for MnCr₂O₄ in FactSage. Nevertheless, the formation sequence of MnCr₂O₄ in the Fe-Cr alloy oxidation can be derived from kurokawa's work [14]. In the present study, the equilibrium diagrams of 100 g Fe-16Cr alloy under various gases were calculated from 500 °C to 1200 °C. They indicated the most possible way of the stainless steel oxidation in various atmospheres. Furthermore, formation sequences and mass change of the compounds in the oxidation of Fe-Cr alloy are suggested.

Fe-16Cr stainless steel was chose to be the typical ferric stainless steels used as interconnects in this calculation. The composition of the Fe-16Cr alloy used in this study is shown in Table 1.

O₂ and H₂O are two of the oxidants of interconnect in operating environment. Oxygen and water are the main components in cathode atmosphere. Wet hydrogen is used as the anode atmospheres. CH4 mixed with different oxidant was also introduced in the calculation.

3 Results and discussion

3.1 Dry oxygen

Figure 1 shows the main produce oxide in the Equilibrium of Fe-16Cr alloys reacted with oxygen at 800 °C. One could see that Cr₂O₃ forms at first. Then the equilibrium phase FeCr₂O₄ forms and Cr₂O₃ disappears with the increase of oxygen introduced into the inhomogeneous reaction. The protective Cr₂O₃ scale prevents Fe-Cr alloys from further oxidization. The deformation of Cr₂O₃ and the formation of iron-contained oxide are indicated that the oxygen transports though the scales more easily, and the oxidization of the metal is faster. It is indicated the material is in failure [23]. Other ferrous anti-oxides appear with the formation of FeCr₂O₄. When O₂ reaches about 1.4 molar, FeCr₂O₄ becomes disintegrating into Fe₂O₃ and Cr₂O₃. Kinds of ferrous oxide coexist after the deformation of Cr₂O₃.

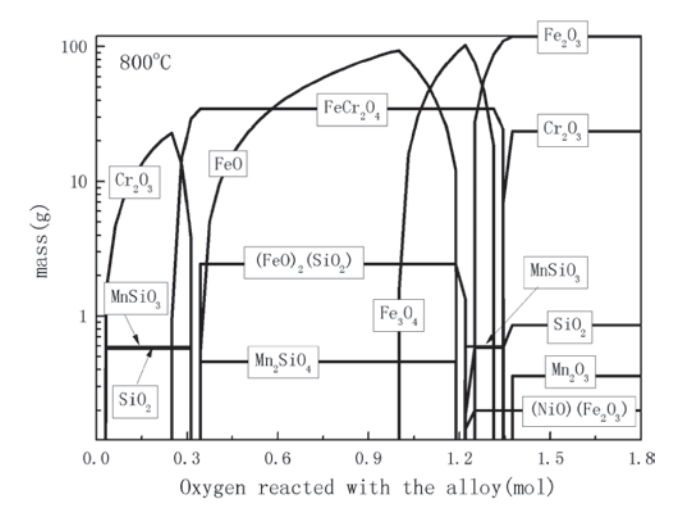


Fig. 1: Equilibrium of oxygen to 100 g Fe-16Cr alloy at 800 °C.

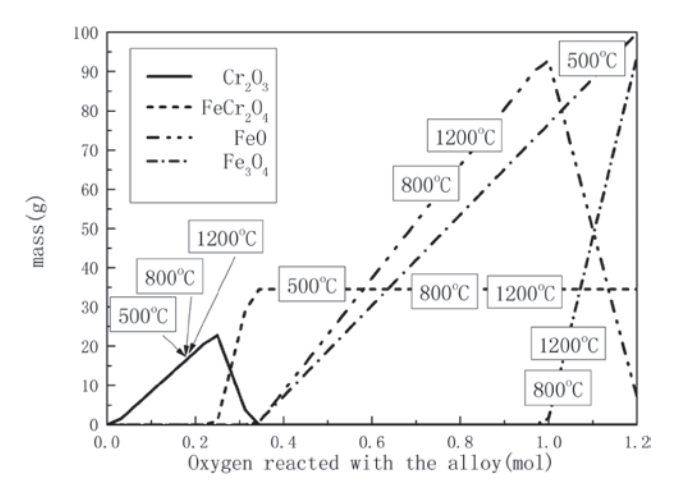


Fig. 2: Equilibrium of oxygen to 100 g Fe-16Cr alloy at different temperature.

SiO₂ and MnSiO₃ appear with the formation of Cr₂O₃ in the calculation results, but the quantities of Mn-oxides and Si-oxides are small. Silicon was also found in the initial oxide scale in the experiment of Brylewski et al. [16].

As Figure 2 shows, ferrous anti-oxides in the equilibrium diagram at 800 °C are very different from it at 500 °C for the reason of the FeO is an unstable phase at high temperature. There are two approaches of Fe oxidizing to Fe₂O₃: 1) Fe \rightarrow Fe₃O₄ \rightarrow Fe₂O₃, which is below 570 °C; 2) $Fe \rightarrow FeO \rightarrow Fe_3O_4 \rightarrow Fe_2O_3$, which is occurred above 570 °C. There was a report that FeO existed in the oxidation process (in the water vapor atmosphere) [24]. The diagrams of 800 °C and 1200 °C are almost the same. It is indicated that the oxidation mechanism is not change during the temperature range in the view of thermodynamics. So the effect of the temperature to the oxidation process is only by the influence to the diffusion rates and

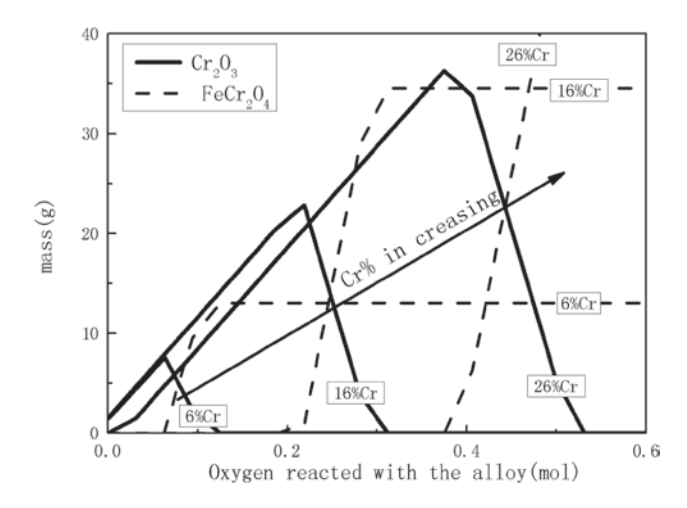


Fig. 3: Equilibrium of oxygen to Fe-Cr alloys with different Cr contents at 800 °C.

the structure of the scales above 570 °C. And the accelerating oxidation experiments above the application temperature of alloy interconnectors are reasonable in the viewpoint of thermodynamics.

Influence of Cr content is considered as shown in Figure 3. Higher Cr content results the higher peak of Cr₂O₃ content. Furthermore, the deformation of Cr₂O₂ and the formation of FeCr₂O₄ are delayed. That means the increase of Cr content in the Fe-Cr alloys is helpful to the oxidation resistance of the alloys.

3.2 Wet oxygen

Water vapor could be introduced to the cathode in wet external environment. As Figure 4 shows, the formation of

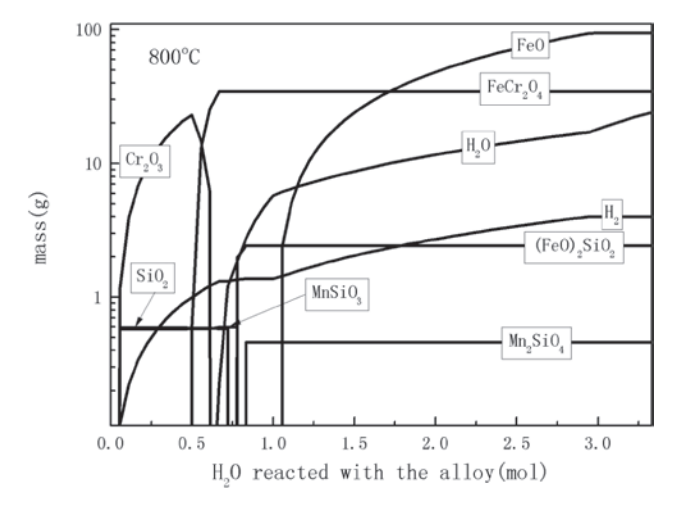


Fig. 4: Equilibrium of pure water vapor to 100 g Fe-16Cr alloy at 800 °C.

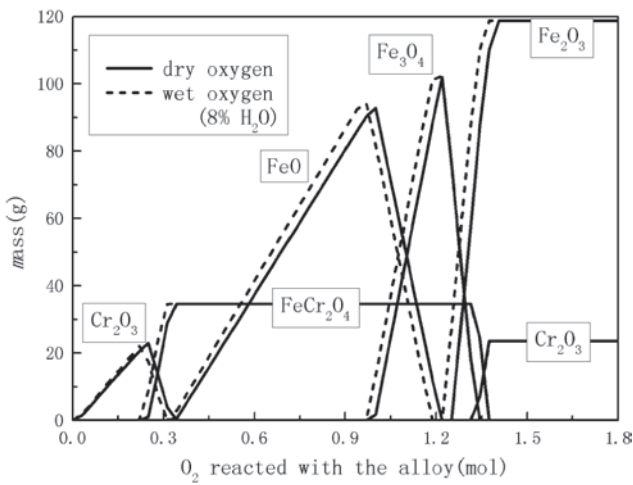


Fig. 5: Equilibrium of dry and wet oxygen to 100 g Fe-16Cr alloy at 800°C

FeCr₂O₄ is start at 0.5 mol H₂O in pure water vapor, instead of at 0.25 mol O₂ in dry oxygen. That means H₂O is a weak oxidant. As a result, FeCr2O4 does not decompose into Fe_2O_3 and Cr_2O_3 in H_2O atmospheres.

The equilibrium diagram of wet oxygen to Fe-16Cr alloy is similar to which of dry oxygen. Nevertheless, the formation of oxides in wet oxygen is earlier than in dry oxygen as shown in Figure 5. The oxidation rate of Crbased alloys in wet oxygen was faster than that in dry oxygen in Reports also [23, 24]. Water vapor plays two different roles in the oxidization of Fe-Cr alloys. Firstly, it is weak oxidant. Secondly, it increases the diffusion of oxygen in dense chromia scales, cause the rapid internal oxidation of alloys [12].

Our calculation results show that the influence of temperature and chromium content in the alloy in wet oxygen ambient are the same as it in dry oxygen. The researchers also founded the corresponding results that the higher Cr content in the alloys was, the longer the protection time in the wet oxygen was [23]. Cr_2O_2 is less stable in the equilibrium calculation results when the content of water vapor in the oxygen is raised. There is a report that the higher water-vapor content, the earlier the initiation of the nonprotective breakaway oxidation [20].

3.3 Wet hydrogen

Alloys can be oxidized in wet hydrogen atmosphere, but the oxidation is slower than which in the air usually [25]. The first oxide appeared in the equilibrium is Cr_2O_2 in wet hydrogen as which in oxidizing atmosphere. As a evidence, the initial dense scale of the alloy was found in the form of chromium oxide in the SEM micrograph [19, 26].

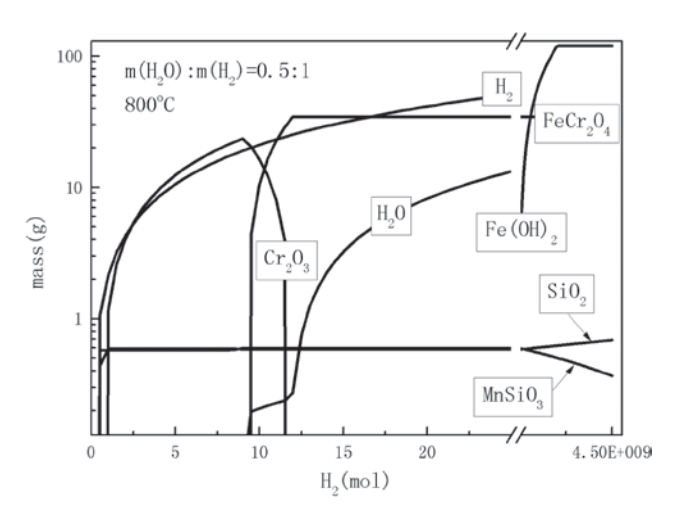


Fig. 6: Equilibrium of H₂O/H₂ (mass ratio: 0.5/1) to Fe-Cr alloys at different temperatures.

As Figure 6 shows, the peak level of Cr₂O₂ and FeCr₂O₄ is the same as Figure 1. That means Cr could be oxidized totally in this atmosphere. Kurokawa et al. observed Cr₂O₃ and FeCr₂O₄ both in the air and H₂O-H₂ atmospheres [14]. It is interesting that the calculation results show that the deformation of Cr₂O₃ and the formation of FeCr₂O₄ are delayed when the temperature is raised.

The finial oxide product is decided by the pressure ratio of H₂O to H₂. The final main solid oxide is change from FeCr₂O₄ to FeO, then to Fe₂O₄, and finally to Fe₂O₂ consequently with the increase of the water vapor mass ratio in the wet hydrogen. Nevertheless, the finial oxide product is $FeCr_2O_4$ even when $m(H_2O):m(H_2)$ reaches to 0.5:1 in the equilibrium. High pressure of Fe(OH)₂ appears in the same condition. Hydrogen is found in the equilibrium diagram, which would results fast oxidization of the alloy.

3.4 Methane

Methane is one of the simplest hydrocarbons. However, the reaction mechanism of it in the SOFC anode chamber is complicated. Carbon, CO₂, and several species produced in the reaction. Carbon deposition is associated with pure methane fuel in the SOFC operation. In addition to reducing carbon formation, oxygen, CO2, or H2O was co-feed in the fuel stream [27, 28]. The oxidation of the interconnect material is associated with the mixtures feeding. Cr₂O₃ and spinel oxides products were found in the alloy reaction with CH₄-H₂O gas [17, 22, 29]. But there are not plenty of studies about the oxidation of alloy in methane containing atmosphere.

Methane is assumed to be introduced in to react with 16Cr stainless steel with a certain amount of CO₂, H₂O or O₂ in the calculation. The equilibrium results are compared in Figure 7. Pure methane results no oxidation, but carburization and carbon deposition. Both of the CO₂, H₂O or O₂ co-feed with methane result the oxidation of the stainless steel. Carbon deposit and carburization is associated with the oxidization in oxidant contained atmosphere. And carburization may results the degradation of the interconnect [15]. Chromium carbide forms at first in the corrosion of Fe-16Cr alloy. Cr₄C reacts with CO₂ to product Cr₃C₂. At the same time, Cr₂O₃ and C form with the deformation of the chromium carbide.

The order of compounds formation is $Cr_{4}C \rightarrow Cr_{3}C_{2} \rightarrow$ $Cr_2O_3 \rightarrow FeCr_2O_4$. The formation and deformation of the Cr₄C lasts short in the equilibrium diagram. With the transformation of the Cr₄C to Cr₃C₂, Carbon deposition generates. Then the Cr₂O₃ formats and Cr₄C disappears. FeCr₂O₄ is the final oxide. So one could see that methane introduced with oxygen will result the oxidation of metallic interconnect. So do the CO₂ and H₂O.

4 Analyses of experimental results

The sample used in the present study was 16Cr stainless steel sheet, and cut into $21 \times 42 \times 1.3$ mm. The surface of each sample was well-polished through 2000 mesh SiC abrasive paper. In a typical experiment, the sample was hanged into a vertical furnace by a Al₂O₂ stick, which was connected to a balance to detect the weight change during the experimental process. Pure air, moist air as well as moist argon gas were introduced in to the reactor respectively. The thermo-gravimetric measurement was accelerated by rising the temperature to 1000 °C. After oxidation corrosion, the microstructure of the sample was analyzed by scanning electron microscope (SEM, CARL ZEISS EVO MA 10/LS 10 JS) with energy dispersive spectrum (EDS, Thermo NORAN System).

The EDS results of alloy oxidized scale at the initial exposure time were detected. The external face of the scale contained Cr: 21.57; Mn: 12.30; O: 66.12. While the internal face of the scale contained Cr: 61.87; O: 38.13. The oxides are supposed to be MnCr₂O₄ and Cr₂O₃ by the EDS results. Many of the former investigations observed MnCr₂O₄, Cr₂O₃ and few FeCr₂O₄ in the initial oxidation process also [16, 30]. Ferrous rich oxides, such as FeO, Fe₃O₄ and Fe₂O₃ formed after the Cr₂O₃ layer could not protected the alloy from oxidization [11, 12].

An EDS result of the cross section of the oxidized Fe-16Cr alloy at 1000 °C in pure air for about 40 min is shown in Figure 8. The outward side of the oxide scale in Figure 8 was ferrous oxide; but near the interface of the oxide scale and the alloy, high Cr content indicated there

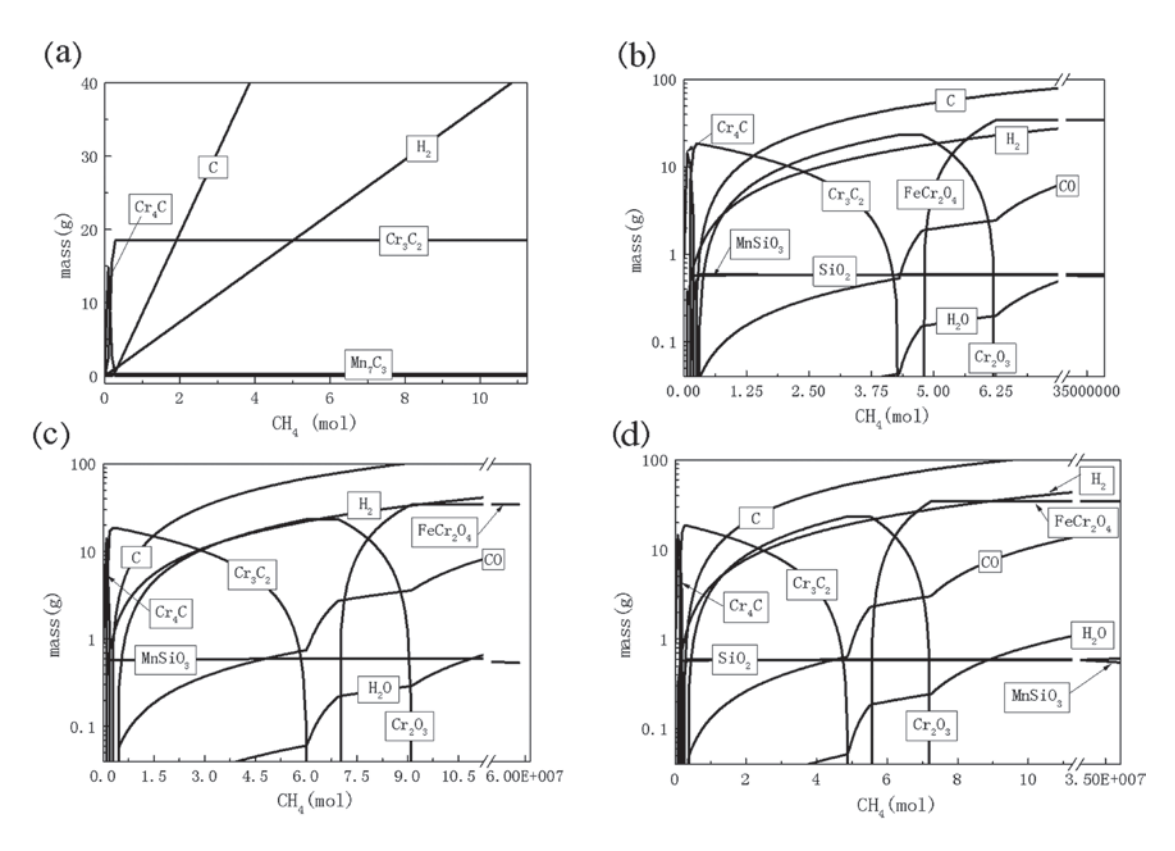


Fig. 7: Equilibrium of (a) pure CH_4 , (b) CH_4 with O_2 (m(O_2):m(CH_4) = 0.12:1), (c) CH_4 with CO_2 (m(CO_2):m(CH_4) = 0.12:1), (d) CH_4 with CO_2 (m(CO_2):m(CO_2):m(

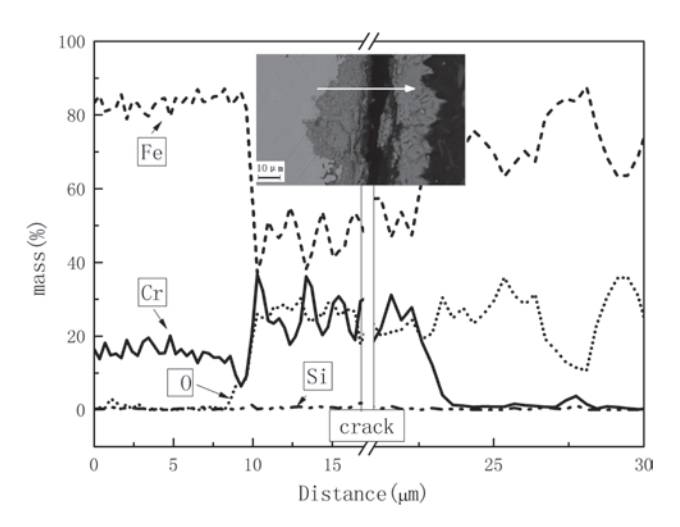


Fig. 8: Elements contents of the cross section of oxidized Fe-16Cr alloy exposure in dry air at 1000 $^{\circ}$ C for about 40 min obtained by EDS.

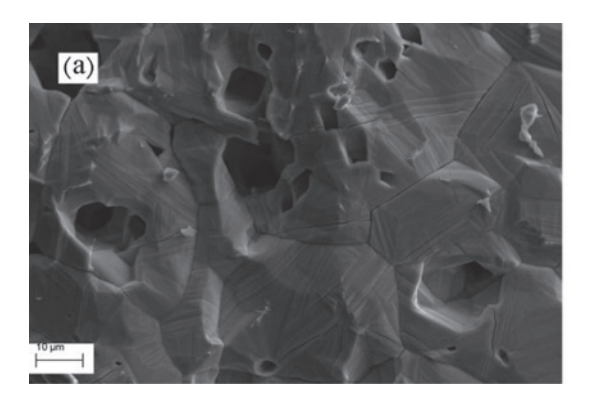
was ${\rm FeCr_2O_4}$. As the EDS and SEM results shown, the formation sequence of oxides is corresponding to the thermodynamic calculation.

The SEM photos of the interface of the oxide scale which was oxidized in wet air (1.2vol% H_2O in air) at 1000 °C is shown in Figure 9(a), sizeable holes and coarser

grains were found at the interface of the scale formed in the wet air compared with Figure 9(b). It suggested that different ways of oxide scale developing. The looser oxide scale compared to the dry air results more quick oxygen diffusion into the fresh alloy interface under the scale. So a quicker oxidation rate will be shown. The formation of hydrogen in the calculation results as Figure 4 shown would be one of the reasons to change the topography of oxide scales.

The mass gain of 16Cr stainless steel in various atmospheres at 1000 °C is given in Figure 10. A slow initial stage to a quick mass gain stage is the sign of the Cr-based alloy oxidation. At the first stage, $\rm Cr_2O_3$ protected the alloy defined the oxidization. But when the Fe rich oxides formed (Figures 1 and 4), the oxidization process was accelerated.

The oxidation of Fe-16Cr alloy in pure argon indicated that there was a little of oxygen in the furnace. But it had little impact the analysis of the experimental results. The transfer time of the first slow oxidation stage to the last quick oxidation stage of the reaction in $\rm H_2O$ was later than it in the dry air atmosphere. However, the reaction rate of the alloy oxidation in the $\rm H_2O$ was faster than it in the dry air. The complicated kinetic phenomenon is the combined effect of thermodynamics and diffusion. The transfer time



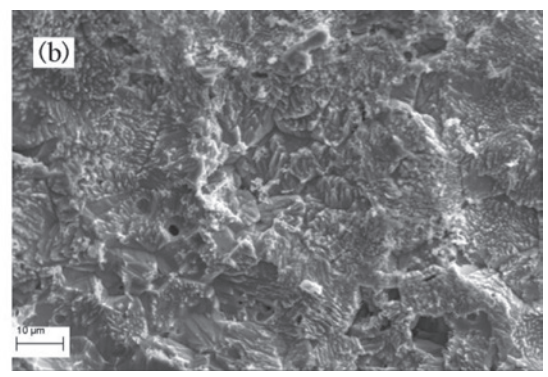


Fig. 9: The SEM micrographs of the Fe-16Cr alloy oxide scale at 1000 °C for 24 h: (a) the internal interface of the scale in H_2O -air (0.001 μ L liquid water pumped into 100 ml air, (b) the internal interface of the scale in air.

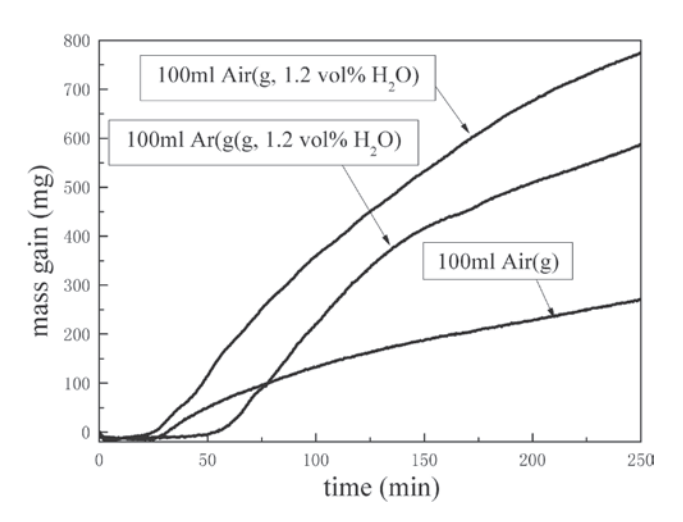


Fig. 10: The mass change curves of Fe-16Cr alloy at 1000 $^{\circ}$ C in different atmospheres.

was move ahead finitely by co-feeding about 1.2vol% $\rm H_2O$ into 100 ml dry air. But the oxidation rate of the second stage increased distinctly.

In Othman's work [12], an obvious change of the main contents in oxide scales of Fe-9Cr alloy was found. The oxides changed from Chromite to ferriferous oxides with the increase of water vapor in the oxygen. It indicated that the oxidation process is accelerated by the co-feed water vapor in oxygen atmosphere. Thermodynamic contribution is one of the reasons to the phenomenon.

5 Conclusions

 The equilibriums of Fe-16Cr alloy at anode/cathode gases were calculated and confirmed by experiment results carried out in our experiments and adequate previous reports. The results obtained in this study show that the thermodynamic diagram in this form

- could be used for deeper insight into the mechanism of the interconnect corrosion.
- 2. The oxides produced in the equilibrium are varying with different amount of gases, atmospheres and temperatures. The order of the solid oxides generation is always $\text{Cr}_2\text{O}_3 \rightarrow \text{FeCr}_2\text{O}_4 \rightarrow \text{FeO} \rightarrow \text{Fe}_3\text{O}_4 \rightarrow \text{Fe}_2\text{O}_3$, but which ferrous oxide exists or not is decided by the oxygen practical pressure. Cr_2O_3 is the most important oxide to protect the alloy form failure. High Cr content in the alloy and low oxygen practical pressure are both advantageous to this scale.
- 3. Carbon deposition and carbonization will happen in carbonic atmospheres. The main carbides are ${\rm Cr_3C_2}$ and ${\rm Cr_aC}$.

Acknowledgments: The authors thank Kun-shan Hua-Tsing Power Co. for material supply and valuable suggestion.

This work is supported by National Program on Key Basic Research Project of China (Grant No. 2012CB215405), National Nature Science Foundation of China (No. 51104013, No. 51174022), and SRF for ROCS, SEM (No. 44) as well as the state key laboratory of advanced metallurgy.

Received: October 19, 2013. Accepted: November 15, 2013.

References

- [1] J. Wu and X. Liu. J. Mater. Sci. Technol., 26(2010), pp. 293–305.
- [2] P. Piccardo, R. Amendola, S. Fontana, S. Chevalier, G. Caboches and P. Gannon. J. Appl. Electrochem., 39(2009), pp. 545–551.
- [3] J. W. Fergus. Mater. Sci. Eng. A, 397(2005), pp. 271–283.
- [4] W. Z. Zhu and S. C. Deevi. *Mater. Sci. Eng. A*, 348(2003), pp. 227–243.

- [5] Z. Yang, K. S. Weil, D. M. Paxton and J. W. Stevenson. J. Electrochem. Soc., 150(2003), pp. A1188-A1201.
- [6] A. Srisrual, S. Coindeau, A. Galerie, J. P. Petit and Y. Wouters. Corros. Sci., 51(2009), pp. 562-568.
- [7] Y. Li, J. Wu, C. Johnson, R. Gemmen, X. M. Scott and X. Liu. Int. J. Hydrogen Energy, 34(2009), pp. 1489-1496.
- [8] J. Hammer, S. Laney, R. Jackson, K. Coyne, F. Pettit and G. Meier. Oxid. Met., 67(2007), pp. 1-38.
- [9] M. Molinelli, D. Larrain, N. Autissier, R. Ihringer, J. Sfeir, N. Badel et al. J. Power Sources, 154(2006), pp. 394-403.
- [10] L. Jian, P. Jian, H. Bing and G. Xie. J. Power Sources, 159(2006), pp. 641-645.
- [11] B. Pujilaksono, T. Jonsson, H. Heidari, M. Halvarsson, J. E. Svensson and L. G. Johansson. Oxid. Met., 75(2011), pp. 183-207.
- [12] N. Othman, J. Zhang and D. Young. Oxid. Met., 73(2010), pp. 337-352.
- [13] P. Jian, L. Jian, H. Bing and G. Xie. J. Power Sources, 158(2006), pp. 354-360.
- [14] H. Kurokawa, K. Kawamura and T. Maruyama. Solid State Ionics, 168(2004), pp. 13-21.
- [15] Z. Zeng and K. Natesan. Solid State Ionics, 167(2004), pp. 9-16.
- [16] T. Brylewski, J. Dabek and K. Przybrlski. J. Therm. Anal. Calorim., 77(2004), pp. 207-216.
- [17] T. Horita, Y. Xiong, K. Yamaji, N. Sakai and H. Yokokawa. J. Power Sources, 118(2003), pp. 35-43.

- [18] T. Horita, Y. Xiong, K. Yamaji, N. Sakai and H. Yokokawa, Proceedings of 5th European Solid Oxide Fuel Cell Forum, 2002, pp. 401-408.
- [19] T. Brylewski, T. Maruyama, M. Nanko and K. Przybylski. J. Therm. Anal. Calorim., 55(1999), pp. 681-690.
- [20] K. Honda, T. Maruyama, T. Atake and Y. Saito. Oxid. Met., **35**(1992), pp. 347-363.
- [21] H. Kurokawa. Solid State Ionics, 168(2004), pp. 13-21.
- [22] T. Horita, K. Yamaji, Y. Xiong, H. Kishimoto, N. Sakai and H. Yokokawa. Solid State Ionics, 175(2004), pp. 157-163.
- [23] S. Jianian, Z. Longjiang and L. Tiefan. Oxid. Met., 48(1997), pp. 347-356.
- [24] E. Essuman, G. Meier, J. Żurek, M. Hänsel and W. Quadakkers. Oxid. Met., 69(2008), pp. 143-162.
- [25] K. Huang, P. Y. Hou and J. B. Goodenough. Solid State Ionics, **129**(2000), pp. 237-250.
- [26] T. Brylewski, M. Nanko, T. Maruyama and K. Przybylski. Solid State lonics, 143(2001), pp. 131-150.
- [27] M. Pillai, Y. Lin, H. Zhu, R. J. Kee and S. A. Barnett. J. Power Sources, 195(2010), pp. 271-279.
- [28] E. S. Hecht, G. K. Gupta, H. Zhu, A. M. Dean, R. J. Kee, L. Maier et al. Appl. Catal. A, 295(2005), pp. 40-51.
- [29] T. Horita, Y. Xiong, H. Kishimoto, K. Yamaji, N. Sakai and H. Yokokawa. J. Power Sources, 131(2004), pp. 293-298.
- [30] T. Brylewski, M. Nanko, T. Maruyama and K. Przybylski. Solid State Ionics, 143(2001), pp. 131-150.